Dyes and Pigments 92 (2012) 1278–1284

Contents lists available at SciVerse ScienceDirect

Dyes and Pigments

journal homepage: www.elsevier.com/locate/dyepig

Sulfanilic acid-modified P25 TiO_2 nanoparticles with improved photocatalytic degradation on Congo red under visible light

Hong-xu Guo[a,*], Kai-li Lin[b], Zi-shan Zheng[a], Fei-bin Xiao[a], Shun-xing Li[a]

[a] Department of Chemistry & Environmental Science, Zhangzhou Normal University, Zhangzhou 363000, PR China
[b] Shanghai Institute of Ceramics, Chinese Academy of Sciences, 1295 Dingxi Road, Shanghai 200050, PR China

ARTICLE INFO

Article history:
Received 18 May 2011
Received in revised form
5 August 2011
Accepted 7 September 2011
Available online 21 September 2011

Keywords:
P25 TiO_2
Sulfanilic acid
Surface modification
Congo red
Photodegradation
Visible light

ABSTRACT

Visible-light-induced titania/sulfanilic acid nano-composite photocatalysts were prepared and characterized by FTIR, XPS, UV-vis, XRD, and SEM. The results indicate that the formation of Ti–O–S bonds after the modification of P25 TiO_2 nanoparticles with sulfanilic acid ligands extends the photoresponse of the photocatalyst from the UV to the visible range. The photocatalytic activity of the nano-composite photocatalyst was examined by degrading Congo red under visible light, in which its effecting factors such as irradiation time, catalyst dosage, solution pH and the addition of H_2O_2, were investigated in detail. The possible mechanism of photocatalytic degradation under visible irradiation has been also presented.

1. Introduction

In the last decade, much attention has been paid to the eradication of various environmental pollutants such as dyes, pesticides, detergents, and volatile organic compounds from wastewater [1–4]. Traditional physical techniques, which include adsorption on activated carbon, reverse osmosis, coagulation by chemical agents, and ion exchange on synthetic adsorbent resins, have been used for the removal of dye pollutants [5,6]. However, these methods only succeed in transferring organic pollutants from water to the other phase. Further, secondary pollution is created, which entails additional and costly solid-waste treatment and regeneration of the adsorbent. Therefore, an alternative to conventional methods is needed. In this regard, a typical alternative method is semiconductor photocatalyst-assisted advance oxidation processes. These are based on the generation of reactive species such as hydroxyl radicals (•OH) that can oxidize a broad range of organic pollutants quickly and non-selectively [7]. Due to its high chemical stability, non-toxicity, high photocatalytic activity to oxidize pollutants in air and water, and relative low price, TiO_2 has been widely used as a photocatalyst in recent decades [8]. However, its application is limited because of its narrow photocatalytic region (near-ultraviolet region) and small fraction (<5%) absorption of incident solar irradiation and indoor light, which results from its relatively large band gap (3.2 eV). In the enhancement of the photoresponse of TiO_2 from the UV to the visible range without decreasing photocatalytic activity, surface modification and dye sensitization have been proven as effective methods as demonstrated by a number of studies [9–12].

The modification of the TiO_2 surface with noble metals such as Ag [13], Pd [14], Au [15], and Pt [16], as well as anion-doping with N [17,18] is well established and is in fact one of the most effective ways to improve TiO_2 photocatalytic activity in the photocatalytic degradation of organic pollution under visible light irradiation. However, the use of noble metals is costly, thereby hindering its practical application. Therefore, there is a need for the development of efficient and cheap co-catalysts as alternatives to noble metals.

Recently, the modification of TiO_2 nanoparticles with organic chelating ligands has been a key research interest because it not only induces dramatic changes in the electrical and optical properties of the nanoparticles, but it also results in the formation of other desirable properties. For example, Cozzoli et al. prepared organic-capped anatase TiO_2 nanorods at 80 °C, which can be dispersed in organic solvents to form optically clear concentrated solutions because of oleic acid surface modification [19]. The Niederberger group developed a nonaqueous sol–gel method to synthesize water-soluble

* Corresponding author. Tel.: +86 596 2591445; fax: +86 596 2520035.
E-mail address: ghx919@yahoo.com.cn (H.-x. Guo).

0143-7208/$ – see front matter © 2011 Elsevier Ltd. All rights reserved.
doi:10.1016/j.dyepig.2011.09.004

dopamine-functionalized anatase TiO_2 nanoparticles [20]. Tahir et al. also prepared dopamine-functionalized rutile TiO_2 nanorods *via* a hydrothermal method [21]. Wang et al. developed an *in situ* chemical oxidative polymerization method in hydrochloric acid solutions to synthesize TiO_2 nanoparticles modified by polyaniline. These nanoparticles exhibit significantly higher photocatalytic activity than neat TiO_2 on the degradation of phenol aqueous solution under visible light irradiation [22]. Zhang et al. synthesized TiO_2 nanorods with enhanced photocatalytic activity *in situ* functionalized with L-hydroxyproline [23]. The Mu group recently prepared a new $C_{60}(CHCOOH)_2$-modified P25 TiO_2 photocatalyst, in which C_{60} is bound chemically to the surface of P25. The photocatalytic reduction activity of the modified P25 for Cr(VI) ions in an aqueous solution can be enhanced significantly [24].

Degussa P25 is a commonly used formulation of TiO_2, which consists of a mixture of anatase (70%) and rutile (30%) mineral phases. This chemical has been proven to be particularly active in oxidizing organic compounds and is frequently used as a representative mixed-phase titanium catalyst, as it displays greater photoactivity compared with single-phase catalysts [25,26]. In addition, commercially available, light sensitive sulfanilic acid (SA) is widely used as small molecular catalysts in the asymmetric synthesis of organic compounds [27,28]. On the other hand, hydrothermal synthesis is a very important and promising method for the fabrication of nanoscale materials. It has been well-proven to be suitable for large-scale production and can yield fine particles with a uniform distribution and high dispersion either in polar or non-polar solvents [29,30]. Further, the aqueous solvents used in the process are environmentally acceptable.

In this study, based on the viewpoints mentioned above, a simple and scalable method to prepare novel SA-modified TiO_2 nanoparticles was developed using hydrothermal treatment under 160 °C. The photocatalytic degradation property of Congo red (CR) using TiO_2/SA nanoparticles as the photocatalysts under visible light irradiation was also examined. The photocatalytic activity of the nano-composite photocatalyst was examined by degrading Congo red under visible light, in which its effecting factors such as irradiation time, catalyst dosage, solution pH and the addition of H_2O_2, were investigated in detail. The possible mechanism of photocatalytic degradation under visible irradiation was also presented.

2. Experimental procedure

2.1. Materials and preparation of the TiO_2/SA nanoparticles

Degussa P25 was purchased from Degussa: Hulls Corporation. Sulfanilic acid (AR.) and Congo red (AR.) were obtained from Sigma Chemical Co.(St. Louis, Missouri). All other reagents were used as received and without further purification. Distilled deionized water was used with a resistivity of 18 MΩ cm. The modified TiO_2 nanoparticles with SA (labeled as TiO_2/SA) were prepared from typical hydrothermal treatment as follows. A mixture of TiO_2 (1.598 g, 20 mmol), SA (0.866 g, 5 mmol), cetyltrimethylammonium bromide (CTAB, 0.911 g, 2.5 mmol), and distilled deionized water (65 mL) was sealed in a 100 mL Teflon-lined reactor and heated in an oven at 160 °C for 10 h and then slowly cooled to room temperature. After filtering, the resulting powder was washed with water and ethanol several times to remove the unreacted SA and surfactant CTAB, then dried at 70 °C in a dust-proof environment to obtain a grayish powder of the TiO_2/SA photocatalyst.

2.2. Characterization of the photocatalyst

The infrared spectra on the pellets of the samples mixed with KBr were recorded on a Perkin Elmer Spectrum 2000 FTIR spectrophotometer at a resolution of 4 cm^{-1}. The TiO_2/SA samples were ultrasonically and fully cleaned to remove the SA ligands physically attached to the TiO_2 surfaces before characterization. The concentration of the TiO_2/SA was kept at about 0.25–0.30 wt.%.

A PerkinElmer Lambda 35 UV/vis spectrometer equipped with a labsphere diffuse reflectance accessory was used to characterize the reflectance spectra of the catalysts over a range of 200–700 nm. Labsphere RSA-PE-20 was used as reflectance standard.

The powder X-ray diffraction (XRD) patterns were recorded on a Rigaku D/MAX-RB diffractometer with monochromatized CuKα radiation ($\lambda = 1.5418$ Å). The generator was operated at 40 kV and 25 mA. The samples were scanned at diffraction angles from 10 to 80° at a scanning rate of 0.068°/s; The C, N and S elemental analyses were carried out on a Perkin–Elmer elemental analyzer.

Morphological observations were performed on a field emission scanning electron microscope (FESEM, S-4800, Hitachi, Japan) and linked with an Oxford Instruments X-ray analysis system.

XPS experiments were carried out in an ultrahigh vacuum using ESCALAB Mark II X-ray photoelectron spectroscopy (XPS, VG Scientific, UK) with Mg Kα radiation (1253.6 eV) from the Mg anode source. The high-resolution scans of core-level spectra were recorded with an energy step of 0.05 eV and set to 15 eV pass energy. The binding energy was referenced at 284.6 eV to the C1s peak. Experimental data were deconvolved by Gaussian–Lorentzian mixture peak-fitting software.

The measurements of surface charge density of TiO_2/SA catalyst as a function of pH were performed by a potentiometric titration process with 100.0 mL of a 20.0 g L^{-1} TiO_2/SA aqueous suspension. The TiO_2/SA was protonated by addition of 0.4 mL of a 1.0 mol/L HCl solution firstly. Then this sample was titrated with NaOH diluted. The pH values were obtained with pH meter (Philips PW 9422).

2.3. Evaluation of photocatalytic properties

To examine the photocatalytic degradation of CR, a solution containing a known concentration of dye and TiO_2/SA nanoparticles was prepared and allowed to equilibrate for 30 min in the darkness. The reactor was open to air to ensure enough oxygen in the reaction solution. The suspension pH values were adjusted to the desired level using dilute NaOH and HCl, and then the pH values were measured with pH meter.

The lamp was switched on to initiate the reaction. A 300 W halogen-tungsten lamp with a cutoff filter ($\lambda > 400$ nm) was used as visible-light irradiation source. During irradiation, agitation was maintained to keep the suspension homogeneous, and then this was sampled after an appropriate illumination time. The concentration of the dye in each degraded sample was determined with a spectrophotometer (UV/vis Spectrophotometer, WFZUV-2000) at $\lambda_{max} = 502$ nm and a calibration curve. Using this method, the conversion percentage of CR can be obtained at different intervals. The degree of degradation rate (DR, %) as a function of time is given as follows: $DR/\% = (C_0 - C_t)/C_0 \times 100\%$, where C_0 is the initial concentration of CR, and C_t is the instant concentration in the sample.

3. Results and discussion

3.1. SEM image

Fig. 1 shows the SEM images of the neat TiO_2 and the prepared TiO_2/SA nanoparticles. From the SEM images, we find that the SA-modified TiO_2 does not change significantly the size compared with the neat TiO_2, but obvious aggregation has been observed after hydrothermal treatment. Clearly, the synthesized TiO_2/SA nanoparticle powders were 30–40 nm in size and spherical-like in

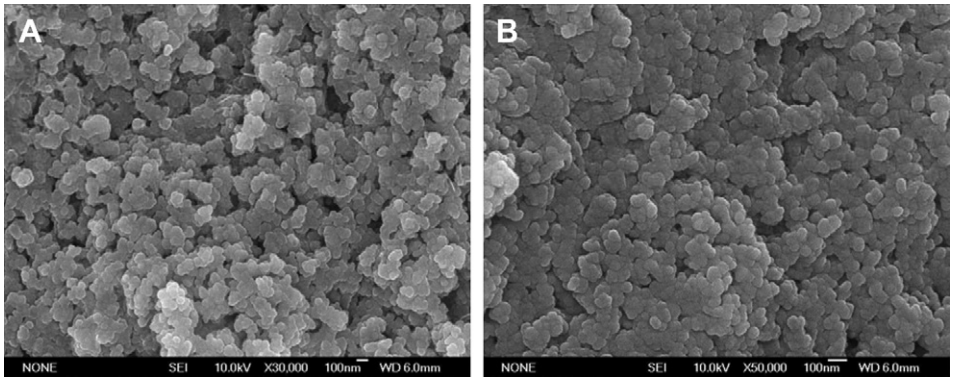

Fig. 1. SEM images of (A) neat TiO_2 and (B) the TiO_2/SA nanoparticles.

shape with a uniform distribution. A higher dispersion increases the specific surface area, which ultimately enhances the photocatalytic performance on the TiO_2/SA nanopowders.

3.2. XRD patterns

Fig. 2 shows the XRD patterns of the neat TiO_2 and TiO_2/SA samples. These patterns can be well indexed to the mixed phases of anatase and rutile. The modification of the TiO_2 particles by SA does not cause any change in their peak positions and shapes compared with the neat TiO_2. This indicates that SA modification through hydrothermal treatment at 160 °C does not change the crystalline structure of TiO_2. Additionally, the amount of grafted SA in the TiO_2/SA measured by elemental analyses (Found C: 5.06, N: 1.03, S: 2.29%) is about 12% (wt.). In the view of the fact that no new diffraction peak appears in the pattern of the TiO_2/SA sample and the content of the SA, it can be concluded that the SA is amorphous in the composite.

The diffraction peaks of the TiO_2/SA sample were slightly sharper than those of neat TiO_2. The mean size of neat TiO_2 and the SA modified particles calculated from Scherrer's formula was 30 and 35 nm, respectively, which agrees well with the SEM image. These results may be attributed to the bonding with SA under the hydrothermal treatment.

3.3. FT-IR analysis

The IR spectroscopy of modified TiO_2 (TiO_2/SA) and neat TiO_2 and SA is shown in Fig. 3. Clearly, the spectrum of the modified TiO_2 nanoparticles (TiO_2/SA) consists of the characteristic peaks of neat TiO_2 and SA ligand. In the spectrum of the TiO_2/SA sample (Fig. 3c), the band at 1633 cm^{-1} is attributed to the stretching mode of O–H bonds on the surface of the TiO_2 nanoparticles, and the bands at 1548, 1423, and 1319 cm^{-1} are the characteristic peaks of the benzene ring which came from organic SA. The wide adsorption band below 950 cm^{-1} is attributed to the vibrations of the inorganic Ti–O and Ti–O–Ti framework bonds in TiO_2. Meanwhile, the peaks at 1035 and 1005 cm^{-1} in the modified TiO_2 sample can be assigned to the S=O asymmetric and symmetric stretching vibrations, respectively. Notably, the band at 708 cm^{-1} can be assigned to the stretching vibration of the S–O bond in the TiO_2/SA spectra, which is larger than that (681 cm^{-1}) of the neat SA sample (Fig. 3b). This indicates that SA can be modified onto the surface of TiO_2 nano-particles through Ti–O–S bonds, which was further confirmed by the XPS results (Fig. 4). The possible graft mechanism of the SA-modified TiO_2 is represented in Scheme 1.

3.4. XPS spectra

XPS characterization of the samples (TiO_2/SA nanoparticles) was also performed to identify the chemical bonding nature of SA on the

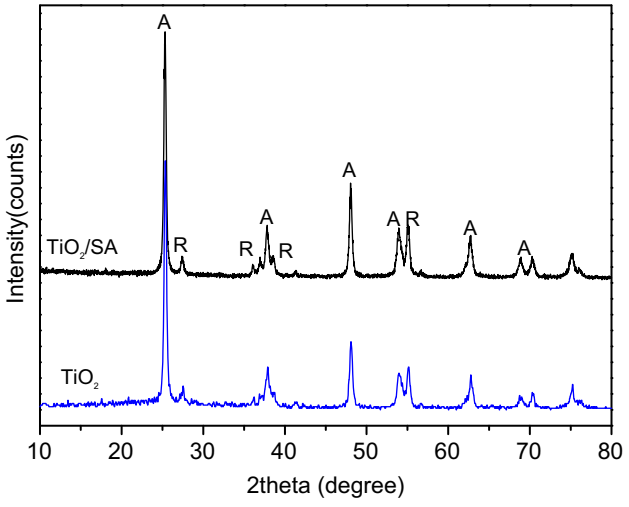

Fig. 2. XRD powder patterns of TiO_2 and TiO_2/SA. A: anatase, R: rutile.

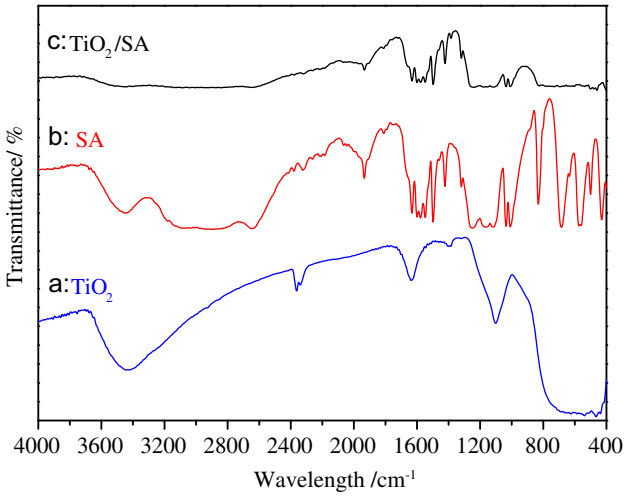

Fig. 3. FTIR spectra of neat TiO_2 (a), SA (b) and modified TiO_2/SA (c).

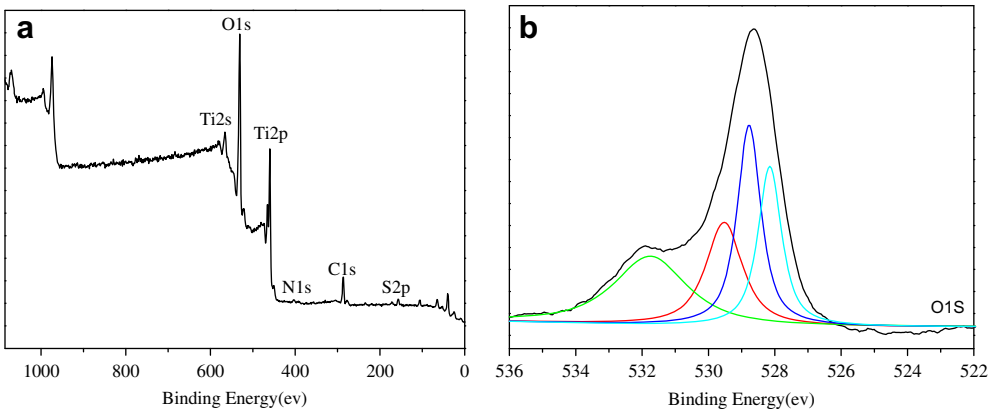

Fig. 4. XPS spectra of survey spectrum (a), and O1s (b) for TiO_2 nanoparticles modified by SA.

TiO_2 nanoparticle surface, as shown in Fig. 4. The typical XPS survey spectrum of the TiO_2 modified by SA reveals that the sample is composed of five elements: Ti, O, C, N, and S (Fig. 4(a)). The XPS Ti 2p core level was observed at binding energies of around 457 eV (Ti $2p_{3/2}$) and 463 eV (Ti $2p_{1/2}$), which is in good agreement with the finding on neat TiO_2. Curve-fitting result suggested that there should exist four kinds of oxygen in SA modified TiO_2, as shown in Fig. 4(b). The peaks at around 528.1, 528.8 and 529.5 eV can be attributed to the oxygen in S=O, Ti–O–Ti and Ti–O–S, respectively [31,32], while the peak at around 531.8 eV can be assigned to surface hydroxyl [33]. The IR and XPS results all confirmed that SA has been successfully bonded to the surface of the TiO_2 nanoparticles by covalent interactions and formed a Ti–O–S bond *via* esterification, which make a strong adsorption as chemical adsorption.

3.5. UV–vis diffuse reflectance spectra

Fig. 5 shows the UV–vis diffuse reflectance spectra of SA and the neat TiO_2 and modified TiO_2/SA nanoparticles. Clearly, there is no absorption above 400 nm for neat TiO_2. However, the modified TiO_2/SA nanoparticle exhibits strong absorption from 400 to 800 nm, which conforms to the grayish color of the powder. Notably, the absorption edge of the TiO_2 modified by SA also red-shifts about 15 nm compared with that of the neat TiO_2 sample. The UV–vis result indicates that some electron interactions between SA and the TiO_2 nanoparticles exist in TiO_2/SA, which might be favorable for the improvement of the photocatalytic activity of TiO_2.

The band gap energies (E_g) of the neat TiO_2 and modified TiO_2/SA nanoparticles were 3.02 and 2.91 eV, respectively, which were obtained from the wavelength values corresponding to the intersection point of the vertical and horizontal parts of the spectra using the following equation: $hc/\lambda = E_g$. E_g is the band gap energy (eV), h is Planck's constant, c is the light velocity (m/s), and λ is the wavelength (nm). The results show that the band gap energy of the TiO_2/SA nanocomposites is apparently lower than that of the neat TiO_2 nanoparticles. Therefore, the TiO_2/SA nanocomposites can be excited to produce much more electron–hole pairs under visible light illumination, resulting in higher photocatalytic activities. This also indicates that SA modification provides an effective approach to extend the absorption of TiO_2 to the visible light range.

3.6. Studies of photocatalytic factors

3.6.1. Effect of irradiation time

Shown in Fig. 6 is the effect of irradiation time on CR degradation. Color of the sample changed to colorless with increasing irradiation time. The experiments showed that absorbance value corresponding to 502 nm increases as irradiation time was increased from 30 to 210 min, concluding that degradation was completed nearly within 210 min. It was observed that decolorization and photodegradation increased with increase in the irradiation time. In order to determine the kinetics of photodegradation, the relationship between $\ln C_t/C_0$ and irradiation time was plotted (as inset in Fig. 6). It was found that the degradation reaction of CR under the catalysis of TiO_2/SA basically obeys to the first order reaction kinetics. For comparison, we also carried out degradation of the CR dye in solution over the neat TiO_2 reference photocatalyst under the same condition, in which only about 12% degradation of CR was observed within 210 min. So the modified TiO_2 nanoparticles show higher photocatalytic activity than that of the neat TiO_2 under visible light irradiation.

3.6.2. Effect of solution pH

The effect of initial solution pH on photocatalytic degradation is generally complex. The solution's initial pH value can directly affect the nature of the charge carried by the catalyst surface and the adsorption behavior of the pollutant in the catalyst surface. In addition, the initial solution pH also further affects the aggregation of the semiconductor catalyst and the band position of the catalyst in the solution.

In order to obtain the pH of the point of zero charge (pzc) for the TiO_2/SA catalyst in the solution, the surface charge density as a function of pH for the photocatalyst was studied, as shown in Fig. 7. The surface charge density σ_o ($C\,m^{-2}$) was calculated from the

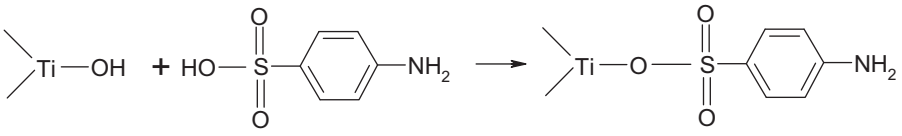

Scheme 1. Schematic of the SA grafted onto the TiO_2 surface by monodentate binding mode.

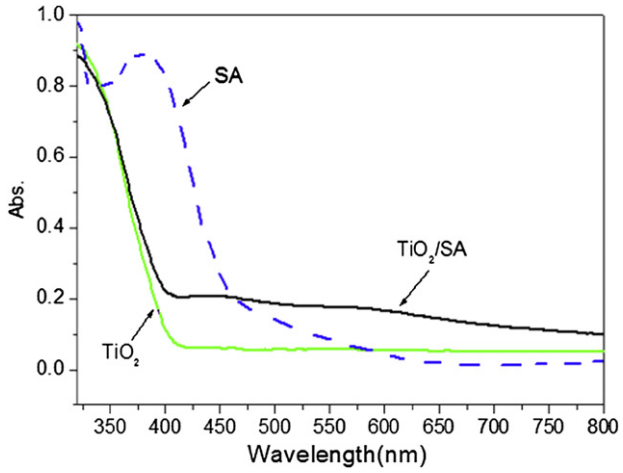

Fig. 5. UV–vis absorbance spectra of the SA, neat TiO_2 and modified TiO_2/SA nanoparticles.

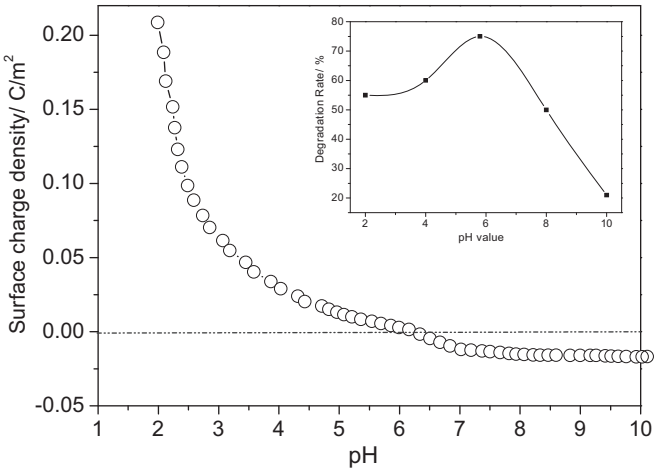

Fig. 7. The variation of surface charge density as function of pH for TiO_2/SA photocatalysts. Inset: Effect of pH value on degradation of CR after 100 min with the TiO_2/SA under visible light. Volume = 100 ml; initial concentration of CR = 40 mg L^{-1}; amount of TiO_2/SA = 1.5 g/L^{-1}.

concentration of H^+ and OH^- ions (mol L^{-1}) adsorbed onto the surface, using the following equation: $\sigma_o = FAm$ ($[H^+]$–$[OH^-]$), where F is the Faraday constant, A the surface area (m^2 g^{-1}) and m is the concentration of the TiO_2/SA catalyst (g L^{-1}). The pH_{pzc} calculated from the results falls at a pH of about 6.3.

The photocatalytic degradation of CR was carried out at different pH values in the range of 2.0–10.0 (Fig. 7 inset) shows that the pH of the solution has a direct effect on the heterogeneous photocatalysis process. High degradation ratios were achieved in acidic and neutral pH regions. This result can be explained that CR molecule with two sulfonic groups ionizes easily in strong acidic media and becomes a soluble CR anion, which can be easily adsorbed to TiO_2/SA particles with positive surface charge. About 75% degradation of CR was observed at pH 6.3 after 100 min. On the contrary, when the solution is in the acidic (pH: 2–4) or alkaline media (pH: 8–10), the degradation rate of CR is lower than that in the optimum pH value. Therefore, the optimum pH for the removal of CR was about pH 6.3.

3.6.3. Effect of catalyst dosage

Fig. 8 shows the effect of TiO_2/SA dosage on the degradation rate of CR at a fixed initial CR concentration (40 mg/L, initial pH value was used) and the same irradiation time (150 min). With an increase in the dosage from 0.5 to 1.0 g/L, the degradation rate apparently increased. A further increase in the dosage resulted in a remarkable decrease in the degradation rate. The optimum weight of catalyst loading was about 1.0 g/L under the given experimental condition. The enhancement in degradation rate as a result of photocatalyst loading is due to the ready availability of total surface area and active sites of the photocatalyst. A reduction in degradation rate was obviously observed at photocatalyst overdose due to the opacity caused by excess photocatalyst clusters. The presence of these clusters then reduces visible light penetration and increases the scattering effect.

3.6.4. Effect of H_2O_2

Hydrogen peroxide, an electron scavenger accepts a photogenerated electron from the conduction band and thus prevents

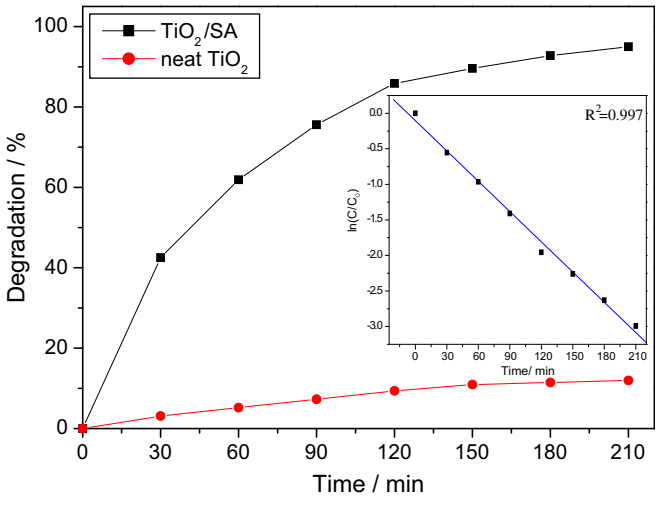

Fig. 6. Photocatalytic degradation curves of CR by TiO_2/SA and neat TiO_2. Inset presents the degradation kinetics of CR using TiO_2/SA by means of plotting $\ln(C/C_0)$ vs. time. Volume = 100 ml; initial concentration of CR = 40 mg L^{-1}; amount of TiO_2/SA = 1.5 g/L^{-1}; initial pH was used.

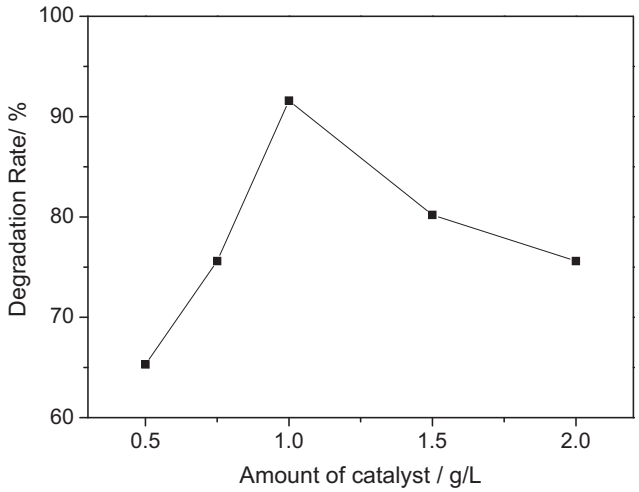

Fig. 8. Relation between amount of catalyst and degradation efficiency of CR; initial concentration of CR = 40 mg L^{-1}, Volume = 100 ml; initial pH value was used; irradiation time = 150 min.

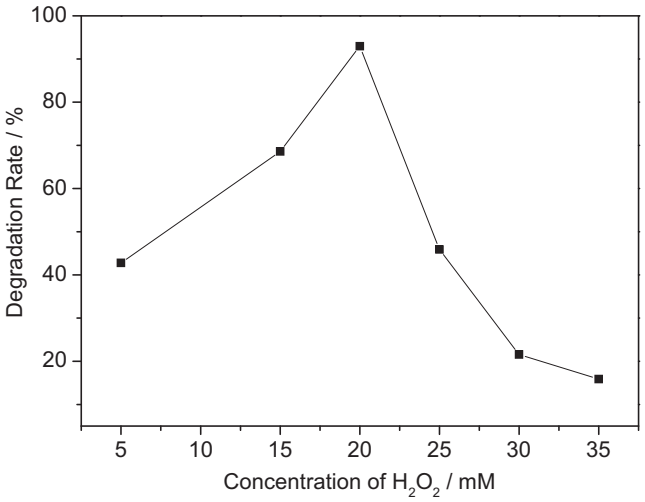

Fig. 9. Effect of dosage of H_2O_2 on degradation of CR after 100 min with the TiO_2/SA under visible light initial concentration of CR = 40 mg L^{-1}; Volume = 100 ml; initial pH was used; amount of TiO_2/SA = 1.5 g/L^{-1}.

electron–hole recombination forming OH• radicals [34]. The effect of H_2O_2 dosage, from 5 to 35 mM, on photodegradation of CR on the TiO_2/SA under visible light was investigated. As shown in Fig. 9, there was an optimal dosage of H_2O_2, 20 Mm, at which the degradation efficiency of CR on the TiO_2/SA attained the height. Below the optimal dosage, the enhancement of degradation by addition of H_2O_2 could be attributed to the increase of reactive hydroxyl radical concentration [35]. While when H_2O_2 presented at higher dosage, the degradation efficiency of CR decreased. This was because the very reactive •OH radicals and valence band holes could be consumed by H_2O_2 itself [36,37].

3.7. Study on the reuse of the photocatalyst

The reuse of the photocatalyst was also studied. The photocatalyst used once under the given condition was dried at 80 °C for 5 h. Then the recovered photocatalyst was reused in the next cycle. As shown in Fig. 10, there is no significant reduction in photoactivity observed when the photocatalyst is used six times for the

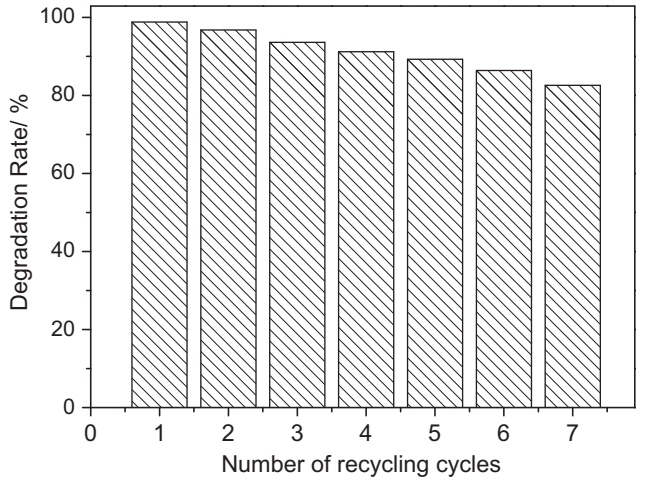

Fig. 10. Effect of number of recycling cycles on the degradation of CR. Initial concentration of CR = 40 mg L^{-1}; Volume = 100 ml; initial pH was used; amount of TiO_2/SA = 1.5 g/L^{-1}; irradiation time = 210 min.

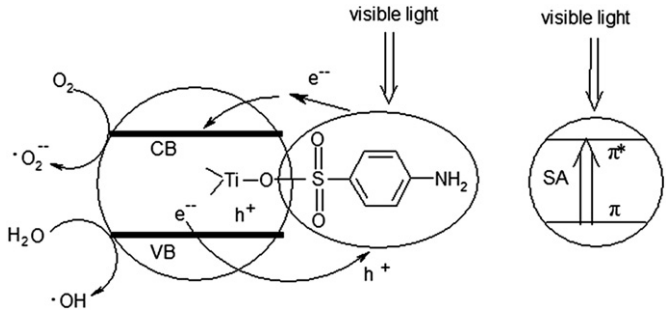

Scheme 2. Mechanism of SA-modified P25 TiO_2 nanoparticles to enhance photocatalytic activity under visible light irradiation.

degradation ignoring the factor of the reduction in quality, indicating that the photocatalytic activity has a good reproducibility and the considerable stability of the photocatalyst under the present conditions.

3.8. Possible visible light-induced photocatalytic mechanism

SA has a maximum absorption at 382 nm and shows strong absorption in the visible light region, whereas TiO_2 itself has an upper absorption edge at about 400 nm, as seen from Fig. 5. The absorption of TiO_2/SA greatly extended to the visible region may be attributed to the synergistic effect between the inorganic and organic composites [38].

The relative energy level of SA (π-orbital and π*-orbital), TiO_2 (conduction band (CB), and valence band (VB)) is shown in Scheme 2. According to the results of the photocatalytic degradation on CR, the mechanism of photocatalytic degradation under visible light irradiation may be interpreted as follows. As a semiconductive material, SA absorbs visible light to induce electron π–π* transition. Afterward, the excited-state electrons are transported from the π-orbital to the π*-orbital. The d-orbital (CB) of TiO_2 and the π*-orbital of SA match well in terms of energy level for the charge transfer [22,24]. With this, the excited-state electrons can be readily injected into the *d*-orbital (CB) of TiO_2 and transferred to the nanocomposite surface to react with oxygen, thus yielding super-oxide radicals $\cdot O_2^-$ subsequently. At the same time, a positive charged hole (h^+) might be formed by electron migration from the TiO_2 valence band to the SA π-orbital, which can react with H_2O in the solution to generate •OH. The super-oxide radical ion $\cdot O_2^-$ and hydroxyl radical •OH are responsible for the degradation of organic compounds. The whole process is shown and described in Scheme 2. Therefore, the whole visible light-induced photocatalytic process of TiO_2/SA can be summarized briefly as follows:

$$TiO_2/SA + h\nu \rightarrow TiO_2/SA^+ + e^- \quad (1)$$

$$e^- + O_2 \rightarrow \cdot O_2^- \quad (2)$$

$$TiO_2/SA^+ \rightarrow TiO_2/SA + h^+ \quad (3)$$

$$h^+\left(H_2O \leftrightarrow H^+ + OH^-\right) \rightarrow H^+ + \cdot OH \quad (4)$$

4. Conclusion

SA-modified P25 TiO_2 visible light photocatalysts have been successfully prepared through hydrothermal treatment. The as-prepared nanoparticles show higher photocatalytic activity than the neat TiO_2 nanoparticles. The active range of the prepared

catalyst is extended from the UV to the visible region, with the formation of Ti–O–S bonds. The photocatalytic activity of TiO_2/SA was examined by degrading CR under visible light, in which its effecting factors (irradiation time, catalyst dosage, solution pH and the addition of H_2O_2) were investigated in detail.

It can be concluded that from the experimental results: (1) The degradation reaction of CR basically obeys to the first order reaction kinetics; (2) The optimum pH for the removal of CR was about 6.3;(3) The optimum weight of catalyst loading was about 1.0 g/L; (4) The optimal dosage of H_2O_2 was 20 mM; (5) The photocatalyst show a good reproducibility and the considerable stability.

Furthermore, the possible visible light-induced photocatalytic mechanism has been proposed. Overall, this study provides an alternative functionalization approach for the effective improvement of the photocatalytic activity of P25 TiO_2 under visible light.

Acknowledgments

This work was supported National Natural Science Foundation of China (nos: 20977074 and 21076174) and the Nature Science of Fujian Education Committee (nos.: JA10205). We also gratefully thank Dr. Wujun Fu (Center for Nanophase Materials Sciences, Oak Ridge National Lab, Oak Ridge, Tennessee, USA) for helpful discussion.

References

[1] Hong CS, Wang Y, Bush B. Kinetics and products of the TiO_2, photocatalytic degradation of 2-chlorobiphenyl in water. Chemosphere 1998;36:1653–67.
[2] Coleman HM, Eggins BR, Byrne JA, Palmer FL, King E. Photocataytic degradation of 17-β- oestradiol on immobilized TiO_2. Appl Catal B Environ 2000;24: L1–5.
[3] Ohko Y, Ando I, Niwa C, Tatsuma T, Yamamura T, Nakashima T, et al. Degradation of bisphenol A in water by TiO_2 photocatalyst. Environ Sci Technol 2001;35:2365–8.
[4] Borker P, Salker AV. Photocatalytic degradation of textile azo dye over $Ce_{1-x}Sn_xO_2$ series. Mater Sci Eng B 2006;133:55–60.
[5] Amat AM, Arques A, Miranda MA, Seguí S. Photo-Fenton reaction for the abatement of commercial surfactants in a solar pilot plant. Solar Energy 2004; 77:559–66.
[6] Lin KL, Pan JY, Chen YW, Cheng RM, Xu XC. Study the adsorption of phenol from aqueous solution on hydroxyapatite nanopowders. J Hazard Mater 2009; 161:231–40.
[7] Kim HG, Borse PH, Choi W, Lee JS. Photocatalytic nanodiodes for visible-light photocatalysis. Angew Chem Int Ed 2005;44:4585–9.
[8] Hernández-Alonso MD, Fresno F, Suárez S, Coronado JM. Development of alternative photocatalysts to TiO_2: challenges and opportunities. Energy Environ Sci 2009;2:1231–7.
[9] Makarova OV, Rajh T, Thurnauer MC. Surface modification of TiO_2 nanoparticles for photochemical reduction of nitrobenzene. Environ Sci Technol 2000;34:4797–803.
[10] Luo YB, Wang XL, Xu DY, Wang YZ. Preparation and characterization of poly(lactic acid) -grafted TiO_2 nanoparticles with improved dispersions. Appl Surf Sci 2009;255:6795–801.
[11] Zaleska A, Grabowska E, Sobczak JW, Gazda M, Hupka J. Photocatalytic activity of boron- modified TiO_2 under visible light: The effect of boron content, calcination temperature and TiO_2 matrix. Appl Catal B Environ 2009;89:469–75.
[12] Akpan UG, Hameed BH. Parameters affecting the photocatalytic degradation of dyes using TiO_2-based photocatalysts: a review. J Hazard Mater 2009;170: 520–9.
[13] Liu Y, Liu CY, Wei JH, Xiong R, Pan CX, Shi J. Enhanced adsorption and visible-light-induced photocatalytic activity of hydroxyapatite modified Ag–TiO_2 powders. Appl Surf Sci 2010;256:6390–4.
[14] Zhu BL, Li KR, Zhou J, Wang SR, Zhang SM, Wu SH, et al. The preparation of palladium- modified TiO_2 nanofibers and their photocatalytic performance. Catal Commun 2008;9:2323–6.
[15] Iliev V, Tomova D, Todorovska R, Oliver D, Petrov L, Todorovsky D, et al. Photocatalytic properties of TiO_2 modified with gold nanoparticles in the degradation of oxalic acid in aqueous solution. Appl Catal A Gener 2006;313: 115–21.
[16] Huang ML, Xu CF, Wu ZB, Huang YF, Lin JM, Wu JH. Photocatalytic discolorization of methyl orange solution by Pt modified TiO_2 loaded on natural zeolite. Dyes Pigments 2008;77:327–34.
[17] Asahi R, Morikawa T, Ohwaki T, Aoki K, Taga Y. Visible-light photocatalysis in nitrogen-doped titanium oxides. Science 2001;293:269–71.
[18] Sakthivel S, Kisch H. Photocatalytic and photoelectrochemical properties of nitrogen-doped titanium dioxide. ChemPhysChem 2003;4:487–90.
[19] Cozzoli PD, Kornowski A, Weller H. Low-temperature synthesis of soluble and processable organic-capped anatase TiO_2 nanorods. J Am Chem Soc 2003;125: 14539–48.
[20] Niederberger M, Garnweitner G, Krumeich F, Nesper R, Colfen H, Antonietti M. Tailoring the surface and solubility properties of nanocrystalline titania by a nonaqueous in Situ functionalization process. Chem Mater 2004;16:1202–8.
[21] Tahir MN, Theato P, Oberle P, Melnyk G, Faiss UK, Janshoff A, et al. Facile synthesis and characterization of functionalized, monocrystalline rutile TiO_2 nanorods. Langmuir 2006;22:5209–12.
[22] Li XY, Wang DS, Cheng GX, Luo QZ, An J, Wang YH. Preparation of polyaniline-modified TiO_2 nanoparticles and their photocatalytic activity under visible light illumination. Appl Catal B Enviro 2008;81:267–73.
[23] Jia HM, Xiao WJ, Zhang LZ, Zheng Z, Zhang HL, Deng F. In situ L-hydroxyproline functionalization and enhanced photocatalytic activity of TiO_2 nanorods. J Phys Chem C 2008;112:11379–84.
[24] Mu S, Long YZ, Kang SZ, Mu J. Surface modification of TiO_2 nanoparticles with a C_{60} derivative and enhanced photocatalytic activity for the reduction of aqueous Cr(VI) ions. Catal Commun 2010;11:741–4.
[25] Hurum DC, Agrios AG, Gray KA. Explaining the enhanced photocatalytic activity of Degussa P25 mixed-phase TiO_2 using EPR. J Phys Chem B 2003;107: 4545–9.
[26] Hurum DC, Gray KA, Rajh T, Thurnauer MC. Photoinitiated reactions of 2, 4, 6 TCP on Degussa P25 formulation TiO_2: wavelength-sensitive decomposition. J Phys Chem B 2004;108:16483–7.
[27] Gulyaiko IV, Kolodyazhnyi OI. Asymmetric synthesis of 1-Hydroxy- 2-alkylphosphonic acids. Russ J General Chem 2005;11:1848–9.
[28] Mak SY, Chen DH. Binding and sulfonation of poly(acrylic acid) on iron oxide nanoparticles: a novel, magnetic, strong acid cation nano-adsorbent. Macromole Rapid Commun 2005;19:1567–71.
[29] Martra G, Coluccia S, Marchese L, Augugliaro V, Loddo V, Palmisano L, et al. Effect of dye-metal complexation on photocatalytic decomposition of the dyes on TiO_2 under visible irradiation. Catal Today 1999;53:695–702.
[30] Luo Y, Ollis DF. Heterogeneous photocatalytic oxidation of trichloroethylene and toluene mixtures in air: kinetic promotion and inhibition, time-dependent catalyst activity. J Catal 1996;163:1–11.
[31] Xie C, Xu ZL, Yang Q, Xue BY, Du YG, Zhang JH. Enhanced photocatalytic activity of titania-silica mixed oxide prepared via basic hydrolyzation. Mater Sci Eng B 2004;112:34–41.
[32] Liu YM, Liu JZ, Lin YL, Zhang YF, Wei Y. Simple fabrication and photocatalytic activity of S-doped TiO_2 under low power LED visible light irradiation. Ceram Inter 2009;35:3061–5.
[33] Xu ZL, Shang J, Liu CM, Kang CL, Guo HC, Du YG. The preparation and characterization of TiO_2 ultrafine particles. Mater Sci Eng B 1999;63:211–4.
[34] Fernández J, Kiwi J, Baeza J, Freer J, Lizama C, Mansilla HD. Orange II photocatalysis on immobilised TiO_2: effect of the pH and H_2O_2. Appl Catal B Environ 2004;48:205–11.
[35] Daneshvar N, Salari D, Khataee AR. Photocatalytic degradation of azo dye acid red 14 in water: investigation of the effect of operational parameters. J Photochem Photobiol A Chem 2003;157:111–6.
[36] Konstantinou IK, Albanis TA. TiO_2-assisted photocatalytic degradation of azo dyes in aqueous solution: kinetic and mechanistic investigations: a review. Appl Catal B Environ 2004;49:1–14.
[37] Mahmoodi NM, Arami M, Limaee NY, Tabrizi NS. Kinetics of heterogeneous photocatalytic degradation of reactive dyes in an immobilized TiO_2 photocatalytic reactor. J Colloid Interf Sci 2006;295:159–64.
[38] Wang DS, Zhang J, Luo QZ, Li XY, Duan YD, An J. Characterization and photocatalytic activity of poly(3-hexylthiophene)-modified TiO_2 for degradation of methyl orange under visible light. J Hazard Mater 2009;169:546–50.